European Journal of Pharmaceutics and Biopharmaceutics 85 (2013) 699–710

Contents lists available at ScienceDirect

European Journal of Pharmaceutics and Biopharmaceutics

journal homepage: www.elsevier.com/locate/ejpb

Research paper

Promoted regeneration of mature blood vessels by electrospun fibers with loaded multiple pDNA-calcium phosphate nanoparticles

Fang Chen [a,1], Huiying Wan [b,1], Tian Xia [c], Xueqin Guo [a], Huan Wang [a], Yaowen Liu [a], Xiaohong Li [a,*]

[a] Key Laboratory of Advanced Technologies of Materials, Ministry of Education of China, School of Materials Science and Engineering, Southwest Jiaotong University, Chengdu, PR China
[b] Institute of Dermatovenereology, Sichuan Provincial People's Hospital, Chengdu, PR China
[c] Department of Pathology, The 452nd Hospital of People's Liberation Army, Chengdu, PR China

ARTICLE INFO

Article history:
Received 30 January 2013
Accepted in revised form 15 July 2013
Available online 24 July 2013

Keywords:
Calcium phosphate nanoparticle
Electrospun fiber
Multiple pDNA delivery
Mature blood vessel
Vascularization
Tissue regeneration

ABSTRACT

Vascularization is one of the capital challenges in the establishment of tissue engineering constructs and recovery of ischemic and wounded tissues. The aim of this study was to assess electrospun fibers with loadings of multiple pDNA to allow a localized delivery for an efficient regeneration of mature blood vessels. To induce sufficient protein expression, a reverse microemulsion process was adopted to load pDNA into calcium phosphate nanoparticles (CP-pDNA), which were electrospun into fibers to achieve a sustained release for 4 weeks. Compared with pDNA-infiltrated fibers, the localized and gradual release of pDNA facilitated cell proliferation, gene transfection, and extracellular matrix secretion and enhanced the generation of blood vessels after subcutaneous implantation. Compared with commonly used pDNA polyplexes with poly(ethyleneimine), CP-pDNA nanoparticles induced significantly lower cytotoxicity and less inflammation reaction after implantation into animals. Fibers with encapsulated nanoparticles containing plasmids encoding vascular endothelial growth factor (pVEGF) and basic fibroblast growth factors (pbFGF) led to significantly higher density of mature blood vessels than those containing individual plasmid. It is suggested that the integration of CP-pDNA nanoparticles with loadings of multiple plasmids into fibrous scaffolds should provide clinical relevance for therapeutic vascularization, getting fully vascularized in engineered tissues and regeneration of blood vessel substitutes.

1. Introduction

The creation of adequate blood vessels remains an essential prerequisite for the establishment of tissue engineering constructs, which require adjacent capillary networks to provide delivery of nutrients and removal of waste products. In addition, the capability to selectively promote accumulation of precursor cells and generation of new blood vessels from existing vessels is a critical consideration in therapeutic angiogenesis for the treatment of ischemic diseases. However, such vascularization networks cannot be generated spontaneously, and vascular regeneration involves a complicated process, which includes the mobilization, adhesion, proliferation, and differentiation of progenitor cells [1]. Thus, it is essential to develop three-dimensional (3D) scaffolds by mimicking the relevant properties of extracellular matrices (ECM) and provide abundant angiogenic growth factors required to initiate and sustain neovascularization.

The soluble growth factors typically have a short half-life, leading to their rapid degradation upon direct administration, which makes it necessary to load them into tissue engineering scaffolds to achieve a localized and sustained release [2]. Anderson et al. covalently bound vascular endothelial growth factor (VEGF) to nanoparticles, leading to an increase in the endothelial cells tube branching and thickness and the total vessel network length compared to soluble growth factors [3]. Anne des Rieux et al. enhanced the efficiency of VEGF by encapsulation into nanoparticles and controlled release from 3D implants to sustain cell infiltration and organization and stimulate blood vessel formation [4]. But one major concern is the maintenance of the structural integrity and biological activity of growth factors during processing and storage of the controlled release systems, and after exposure to enzymatic and acidic microenvironment created by the acidic by-products of polymer degradation [5]. The potential activity loss usually requires high dosages loaded into the delivery system, which creates potential exposure to toxic levels of protein if unexpected dose dumping occurs. The use of plasmid DNA (pDNA) to produce growth factors in transfect cells provides a powerful alternative, is generally advantageous in long-term effects, and has low costs

* Corresponding author. Key Laboratory of Advanced Technologies of Materials, Ministry of Education of China, School of Materials Science and Engineering, Southwest Jiaotong University, Chengdu 610031, PR China. Tel.: +86 28 87634068; fax: +86 28 87634649.
E-mail address: xhli@swjtu.edu.cn (X. Li).
[1] These authors contributed equally to the work.

0939-6411/$ - see front matter © 2013 Elsevier B.V. All rights reserved.
http://dx.doi.org/10.1016/j.ejpb.2013.07.009

compared to purified protein delivery. Although naked DNA achieved gene expression and guided tissue regeneration in porous scaffolds [6], limitations with low gene transfer efficiency and rapid diffusion of pDNA from the scaffold motivated the use of DNA complexes instead of free pDNA. Guo et al. prepared complexes of VEGF-encoded pDNA (pVEGF) with N,N,N-trimethyl chitosan chloride, which were loaded into a bilayer porous collagen–chitosan/silicone membrane as dermal equivalents for treatment of full-thickness burn wounds. The loading of pDNA complexes resulted in a significantly high number of newly formed and mature blood vessels and fast dermal regeneration [7].

Cationic lipids or polymers have previously been introduced to condense pDNA and incubated in tissue engineering scaffolds. Liposomal systems have been frequently applied in vitro, but require strict conditions including correct cell density and components of the culture media, so it is difficult to apply this method in vivo [8]. Poly(ethyleneimine) (PEI) is a widely utilized cationic polymer for nonviral gene delivery, but suffers from noticeable cytotoxicity and immune reactions, thereby reducing the clinical relevance [9]. Calcium phosphate, the major component of hard tissues, exhibits a high binding affinity with pDNA most likely due to interactions between calcium ions and the negatively charged phosphate groups in pDNA, and thus may impart a stabilizing function to certain pDNA structures [10]. One advantage of calcium phosphate as a drug delivery vehicle is that calcium phosphate-pDNA (CP-pDNA) complexes can be carried across cell membrane via ion channel mediated endocytosis [11]. Another major advantage is that calcium phosphate is relatively insoluble at physiological pH, but has increasing solubility in the acidic environments that occur in endosome and lysosome, facilitating the intracellular delivery of pDNA [12]. Curtin et al. incorporated calcium phosphate nanoparticles containing pDNA encoding bone morphogenetic proteins into collagen-based scaffolds, and the osteogenesis was enhanced when using low levels of plasmids demonstrating their innate capacity for promoting bone formation [13].

Electrospun fibers have attracted a great deal of attention, especially in biomedical fields, as scaffolds for tissue engineering and drug delivery because of the similar skeletal structure to ECM, flexible variation in morphology, interconnected pores, and high specific surface area, and have shown to be effective for local and sustained delivery of bioactive signals [14]. To induce sufficient protein production, pDNA was incorporated into electrospun fibers through electrostatic layer-by-layer deposition of polycations and pDNA [15] or surface deposition of pDNA/chitosan nanoparticles [16]. But a significant initial release of pDNA nanoparticles led to high cytotoxicity and short-term gene expression [16]. Alternatively, emulsion electrospinning was initially applied to prepare core–sheath structured fibers with the core-loading of PEI–pDNA polyplexes [17]. The gradual release of pDNA and sufficient expression of growth factors enhanced skin wound healing in diabetic rats [18] and promoted the generation of blood vessels [19]. But significantly low cell viability, strong inflammation, and necrotic tissues were indicated for electrospun fibers with loaded PEI–pDNA polyplexes [19].

This study was aimed to assess biodegradable electrospun fibers with loadings of CP-pDNA nanoparticles to allow a localized delivery for an efficient vascularization. It was indicated that the transfection efficiency of standard preparations of CP-pDNA precipitates decreased over time as the inorganic crystals continued to grow and aggregate, becoming too large for endocytosis by cells [20]. Organic and inorganic additives and multiple-layer structures were then adopted to preserve the small size of calcium phosphate particles and to inhibit their further growth [20]. In the current study, the incorporation of calcium phosphate nanoparticles into electrospun fibers was supposed to maintain the size stability and transfection efficiency over time. Although a variety of growth factors are known to be involved, VEGF and basic fibroblast growth factor (bFGF) are the key mediators of new blood vessel growth which makes them particularly interesting for their use in blood vessel engineering and therapeutic angiogenesis [21]. Therefore, hydroxyapatite (HA) nanoparticles with encapsulated pVEGF and bFGF-encoded plasmid (pbFGF) were synthesized using reverse microemulsions. Electrospun fibers with loadings of the nanoparticles were prepared, and pDNA release was modulated to adapt to the duration for blood vessel regeneration. The cellular behaviors, including cell adhesion, proliferation, transfection efficiency, and ECM secretion, were evaluated in vitro on endothelial cells (ECs) and smooth muscle cells (SMCs). The extent of vascularization and vessel maturation was clarified after subcutaneous implantation into Sprague–Dawley rats via hematoxylin–eosin (HE) and immunohistochemical (IHC) staining.

2. Materials and methods

2.1. Materials and cells

Poly(DL-lactide)–poly(ethylene glycol) (PELA, M_w = 42.3 kDa, M_w/M_n = 1.23) was prepared by bulk ring-opening polymerization of DL-lactide using 10% (wt/wt) of dihydroxyl-poly(ethylene glycol) (PEG, M_w = 6 kDa) as macroinitiator [22]. The pVEGF, encoding fusion protein of VEGF/enhanced green fluorescent protein (eGFP), and pbFGF, encoding bFGF/eGFP fusion protein, were purchased from FulenGen Co. (Guangzhou, China). The plasmids were grown in *Escherichia coli* DH5α using LB growth media, purified using Qiagen Giga kit (Hilden, Germany), and stored in Tris–EDTA buffer (TE, 10 mM Tris–HCl, 1 mM EDTA, pH 8.0) at 4 °C. All the electrophoresis reagents, PEG (M_w = 2, 4, and 6 kDa), PEI (M_w = 25 kDa), bovine serum albumin (BSA), 4′,6-diamidino-2-phenylindole (DAPI), propidium iodide (PI), and bisbenzimide (Hoechst 33258) were procured from Sigma (St. Louis, MO). Protein molecular weight marker and RIPA lysis buffer were from Beyotime Institute of Biotechnology (Shanghai, China). Rabbit antihuman antibodies of collagen I, collagen IV, laminin, α-smooth muscle actin (α-SMA), and β-actin, rabbit anti-mouse antibodies of CD31, collagen IV and α-SMA, goat anti-rabbit IgG-horseradish peroxidase (HRP), IgG-fluorescein isothiocyanate (FITC), and 3,3′-diaminobenzidine (DAB) developer were purchased from Boster Bio-engineering Co., Ltd. (Wuhan, China). All other chemicals were of analytical grade and received from Changzheng Regents Company (Chengdu, China) unless otherwise indicated. Human umbilical vein ECs and human aortic SMCs were from American Type Culture Collection (Rockville, MD) and maintained in Dulbecco's modified Eagle's medium (DMEM, Gibco BRL, Rockville, MD) supplemented with 10% heat inactivated fetal bovine serum (FBS, Gibco BRL, Grand Island, NY).

2.2. Preparation of CP-pDNA nanoparticles

CP-pDNA nanoparticles were prepared following a published report with some modifications [23]. Briefly, two separate microemulsions (A and B) were formed with a cyclohexane/polyoxyethylene octylphenol ether (OP-10)/water system, in which cyclohexane acted as the oil phase and OP-10 was the surfactant. 0.5 mL $Ca(NO_3)_2$ aqueous solution (0.25 M) containing 250 μg pDNA was emulsified into 15 mL cyclohexane containing 10% (v/v) OP-10 by continuous stirring for 1 h to form microemulsion A. Similarly, microemulsion B was formed by emulsification of 0.5 mL $(NH_4)_2HPO_4$ aqueous solution (0.15 M) containing 250 μg pDNA into 15 mL cyclohexane containing 10% (v/v) OP-10. Microemulsion B was slowly added to microemulsion A at the rate of

5 mL/h with continuous stirring, and the mixture was adjusted to pH 9.0 by 1 M ammonia. The resulting solution was stirred for another 1 h and then centrifuged at 15,000 rpm to collect the nanoparticles. The nanoparticles were washed with ethanol three times and lyophilized to obtain CP-pDNA nanoparticles. Empty calcium phosphate (CP) nanoparticles were prepared without pDNA addition in above microemulsions.

2.3. Characterization of CP-pDNA nanoparticles

CP-pDNA nanoparticles were observed by atomic force microscope (AFM, CSPM5000, Beijing, China) after the sample-loaded silicon wafer was air-dried at room temperature. The average size and zeta potential were measured by a Nano-ZS laser particle analyzer (Zetasizer Nano ZS90, Malvern Co., UK). To investigate the crystalline phase of calcium phosphate, CP-pDNA nanoparticles were analyzed using X-ray powder diffraction (XRD, Philips X'Pert PRO, Philips, The Netherlands) employing Cu Kα radiation (45 kV, 40 mA). The diffraction patterns were collected with 2θ ranging from 10° to 60° with a scanning speed of 0.35°/min.

The pDNA loading efficiency was determined by extraction from nanoparticles and quantification with Hoechst 33258 dye. Briefly, CP-pDNA nanoparticles were extracted three times with phosphate buffer solution (PBS) containing 10 mg/mL heparin. The extract was mixed with Hoechst 33258, and the fluorescence intensity was measured by a fluorospectrophotometer (Hitachi F-7000, Japan) at an excitation wavelength of 350 nm and an emission wavelength of 450 nm. The pDNA concentration was obtained using a standard curve from known concentrations of pDNA solutions. The extraction efficiency was calibrated by adding a certain amount of pDNA solution into empty CP nanoparticles along with the same concentration as above and extracted using the above-mentioned process. The encapsulation efficiency indicated the percentage of pDNA encapsulated with respect to the total amount used for particle preparation.

The protective effect of nanoparticles on the structural integrity of pDNA entrapped was determined by DNase I digestion as described previously [17]. Briefly, CP-pDNA nanoparticles were suspended in 100 μL of Tris–EDTA buffer containing 0.3 U DNase I (Takara Company, Dalian, China), using free pDNA and free pDNA-adsorbed empty nanoparticles (CP + pDNA) as control. After incubation at 37 °C for specific time intervals, pDNA was extracted as above, and electrophoresized in 1% agarose gel (Power PacTM Universal, Bio-RAD, Hercules, CA). The gel was finally viewed by a gel documentation system (Bio-RAD, Hercules, CA) to determine the structural integrity of pDNA.

2.4. Cell growth and transfection with CP-pDNA nanoparticles

The viability and transfection levels were examined on ECs and SMCs after incubation with CP-pDNA nanoparticles, using CP + pDNA nanoparticles and PEI–pDNA polyplexes as control. The PEI–pDNA polyplexes were formed by mixing 500 μL of PEI solution (22.3 mM in pH 7.0 PBS) and 500 μL of pDNA solution (1 mg/mL in pH 7.0 PBS) [18]. EC or SMC suspension with a cell density of 5×10^4 cells/mL was seeded in 24-well tissue culture plates (TCP) and incubated for 24 h to allow cell attachment. Cells were treated with nanoparticles containing 1.0 μg pDNA for 48 h, and the cell viability was assayed with cell counting kit (CCK-8, Dojindo Molecular Technologies, Inc., Kumamoto, Japan). Briefly, after removal of particles-containing medium, 400 μL of fresh culture medium was added in each well. Then, 40 μL of CCK-8 was added to each well and incubated for 2 h according to the reagent instruction. An aliquot (150 μL) of incubation medium was pipetted into a 96-well TCP, and the absorbance at 450 nm was measured for each well using a μQuant microplate spectrophotometer (Elx-800, Bio-Tek Instrument Inc., Winooski, VT).

To measure the transfection levels, the culture media were removed after 48 h treatment, and cells were homogenized in a lysis buffer (0.1 M Tris-HCl, 2 mM EDTA, 0.1% Triton X-100). The lysate was centrifuged at 12,000 rpm for 5 min at 4 °C to collect the supernatant. The relative light unit (RLU) was quantified using a fluorospectrophotometer at an excitation wavelength of 493 nm and an emission wavelength of 510 nm. The total protein of the cell lysate was determined by BCA protein assay kit (Pierce, Rockford, IL). Results of pDNA expression were normalized as relative light units per mg of soluble protein (RLU/mg protein). All experiments were performed with $n = 6$.

2.5. Preparation of electrospun fibers with loading of CP-pDNA nanoparticles

The CP-pDNA nanoparticles-loaded fibers were prepared by blend electrospinning as described previously [17]. Briefly, CP-pDNA nanoparticles were suspended into 2.0 mL of acetone containing 500 mg of PELA. The resulting suspension was added in a 5-mL syringe attached to a metal capillary, and a steady flow at 10 mL/h out of the capillary was controlled by a microinject pump (Zhejiang University Medical Instrument Co., Hangzhou, China). The capillary was connected with a high voltage statitron (Tianjing High Voltage Power Supply Co., Tianjing, China), and the applied voltage was set as 20 kV. The electrospinning distance was 15 cm, and fibers were subsequently on deposited on grounded aluminum foil fixed on a plate-type collector. The collected fibers were vacuum dried overnight and stored at 4 °C in a desiccator for further use. Electrospun fibers with entrapment of CP-pVEGF, CP-pbFGF nanoparticles, and both of them were prepared, which were named as Fv, Fb, and Fv-b, respectively. Empty electrospun fibers without pDNA inoculation were also prepared as F_0. PEG with M_w of 2, 4, and 6 kDa was blend with PELA at the ratio of 10% to obtain F2, F4, and F6 fibers, respectively.

In order to visualize the distribution of CP-pDNA nanoparticles in electrospun fibers, pVEGF and pbFGF were labeled with DAPI and PI, respectively. Briefly, DAPI labeling was performed by mixing DAPI solution (10 μg/mL in PBS) with pVEGF in the dark and PI labeling by mixing PI solution (100 μg/mL in PBS) with pbFGF in the dark. The reaction mixture was dialyzed to remove any residual FITC or PI. Electrospun fibers Fv-b with entrapped CP-dapi-pVEGF and CP-pi-pbFGF nanoparticles were prepared as mentioned above.

2.6. Characterization of electrospun fibers

The morphology of electrospun fibers was investigated by a scanning electron microscope (SEM, FEI Quanta 200, The Netherlands) equipped with a field-emission gun (20 kV) and a Robinson detector after 2 min of gold coating to minimize the charging effect. The fiber diameter was measured from SEM images, and the porosity of fibrous mats was determined from the apparent density as described previously [24]. The entrapment of CP-pDNA nanoparticles in electrospun fibers was observed with confocal laser scanning microscopy (CLSM, Leica TCS SP2, Germany). The excitation and emission wavelengths of DAPI were 364 and 454 nm, and those of PI were 535 and 615 nm, respectively. Electrospun fibers were dissolved in dichloromethane, followed by extraction three times with PBS containing 10 mg/mL heparin. The pDNA concentration of the extract was measured as above, and the loading efficiency indicated the percentage of pDNA encapsulated with respect to the total amount used for fiber preparation.

2.7. In vitro pDNA release from electrospun fibers

Electrospun fibrous mats containing CP-pDNA nanoparticles were cut into small squares (1×1 cm^2) with a total mass of about 100 mg and sterilized by electron-beam irradiation using linear accelerator (Precise™, Elekta, Crawley, UK) with a total dose of 80 cGy. The fibrous mats were immersed in 3.0 mL of PBS, pH 7.4, and the suspensions were kept in a thermostated shaking water bath maintained at 37 °C and 100 rpm. At predetermined time intervals, the release buffer was removed for analysis, and fresh PBS was added for continuing incubation. The release buffer was incubated in 10 mg/mL heparin solution, and the amount of pDNA released was detected with Hoechst 33258 dye as described above. The release buffers were electrophoresized in 1% agarose gels to evaluate the structural integrity of pDNA released, using free pDNA incubated in PBS as control.

2.8. Cell growth and transfection on pDNA-loaded fibers

Before cell seeding, 12 mm diameter disks were punched from fibrous mats F_0, Fv, Fb, and Fv-b, fixed by a cell-culture ring with 10 mm of internal diameter as designed by Zhu et al. [24] and sterilized. CP-pDNA nanoparticles infiltrated fibrous mats were prepared by dropping CP-pVEGF, CP-pbFGF nanoparticles, and both of them onto F_0 fibrous mats, which were named as F_0 + v, F_0 + b, and F_0 + v-b, respectively. The fibrous mats were placed into 48-well TCP, and 100 μL ECs or SMCs suspension with a cell density of 2×10^4 cells/mL was seeded, which were maintained for 4 h to make cells diffuse into and adhere to the scaffold before the addition of 900 μL of culture media into each well. The cell viability tests were repeated on days 1, 3, 5, and 7 after cell seeding by CCK-8 as described above.

The transfection levels of pDNA released from fibers were measured for 28 days. ECs and SMCs were removed from fibrous scaffolds by trypsinization after 7 days of culture, and an almost complete removal was indicated by SEM observation. Another batch of cells was seeded on the recovered fibrous mats and incubated for another 7 days, and the cell depletion and inoculation processes were repeated till the total culture time of 28 days. Fibrous mats were harvested at predetermined time intervals, washed with PBS three times, and homogenized in a lysis buffer. The GFP expression of the lysate was measured and normalized into RLU/mg protein as described above.

2.9. ECM secretion of cells on pDNA-loaded fibers

The secretion of collagen IV and laminin by ECs and that of collagen I and α-SMA by SMCs were examined by immunofluorescent staining. Briefly, cells-loaded on fibrous mats were washed with PBS, fixed with 4% paraformaldehyde, and permeabilized with 0.1% Triton X-100 solution in PBS. Fibrous mats were incubated with rabbit antihuman antibodies of collagen I, collagen IV, laminin, or α-SMA for 2 h at 37 °C. Then, fibrous mats were washed three times with PBS, incubated for another 1 h at room temperature with secondary FITC-conjugated antibody for 1 h, and then washed three times with PBS. Finally, fibrous mats were mounted and observed using CLSM with the excitation and transmission wavelength of 488 and 535 nm, respectively.

Western blot was used to determine collagen IV secretion by ECs and α-SMA by SMCs. Briefly, cells on fibrous mats were homogenized in RIPA lysis buffer, and total proteins were collected by centrifuging at 12,000 rpm at 4 °C. The total protein of the cell lysate was determined by BCA protein assay kit. The cell lysate was then mixed with loading buffer (40 mM Tris-HCl, 1% SDS, 50 mM DTT, 7.5% glycerol, 0.003% bromophenol blue) and then subjected to electrophoresis on 10% SDS–PAGE gel at 100 V, followed by transfer to PVDF membrane (Millipore Corp., Bedford, MA). After blocked with 5% BSA for 2 h at room temperature, the membrane was washed and incubated with rabbit antihuman antibodies of collagen IV or α-SMA for 1 h at room temperature and kept at 4 °C overnight. Membranes were then washed three times with PBS containing 0.05% Tween 20 and reacted with secondary HRP-conjugated antibody for 1 h. Antigen-antibody complexes were visualized by DAB developer. Expression of β-actin was used as protein loading control.

2.10. Subcutaneous implantation of pDNA-loaded fibers

The acceleration of angiogenesis was assessed after subcutaneous implantation, and all animal procedures were approved by the University Animal Care and Use Committee. Male SD rats, from Sichuan Dashuo Biotech Inc. (Chengdu, China), weighing 100 to 120 g, were denuded on the back with 8% Na_2S aqueous solution. The rats were anesthetized by intraperitoneal injection of pentobarbital sodium at a dosage of 30 mg/kg, and four subcutaneous pockets were made on both sides on the back. The sterilized electrospun fibrous mats were rolled into a cylindrical shape and were implanted into the subcutaneous pockets before suturing the incisions. CP-pDNA nanoparticles-loaded fibrous mats Fv, Fb, and Fv-b, CP-pDNA nanoparticles-infiltrated fibrous mats F_0 + v, F_0 + b, and F_0 + v-b, and empty fibers F_0 were tested.

2.11. Characterization of blood vessel formation

The implants with surrounding tissues were retrieved at weeks 1, 2, and 4 after operation. One part of the tissues retrieved was frozen and cut into 4 μm sections for HE staining to evaluate the fiber residuals, inflammatory reaction, and blood vessel formation. HE-stained sections were observed with a light microscope (Nikon Eclipse E400, Japan). Another part of the tissues retrieved was fixed in formalin, paraffin-embedded, sectioned into 5 μm slices for IHC staining of CD31, collagen IV and α-SMA. Briefly, tissue sections were incubated with 3% H_2O_2 for 10 min to inactivate endogenous peroxidase, followed by exposure to microwave heating in 10 mM citrate buffer solution (pH 6.0) to recover antigens. Non-specific binding sites were blocked with 5% BSA in Tris-buffered saline for 20 min, and the sections were incubated with primary antibodies at 4 °C overnight. Then, the slides were incubated with biotinylated secondary antibody for 20 min, followed by incubation with streptavidin-HRP for 20 min. The antibody binding sites were visualized by incubation with a DAB–H_2O_2 solution. The slides were counterstained for 1 min with hematoxylin and then dehydrated with sequential ethanol for sealing and microscope observation. A minimum of 10 individual microscopic images were randomly selected from 3 different slides of each group. Collagen IV and α-SMA positive vessels with morphological circumference of staining of 1 or more cells were counted, while positive staining with single dot was not counted as capillary vessels [25]. The blood vessel density was normalized to tissue area (number of vessels/mm^2).

2.12. Statistics analysis

The values were expressed as means ± standard deviation (SD). Whenever appropriate, two-tailed Student's *t*-test was used to discern the statistical difference between groups. A probability value (p) of less than 0.05 was considered to be statistically significant.

3. Results and discussion

3.1. Characterization of CP-pDNA nanoparticles

The non-immunogenic response, non-toxic degradation products, and pH-dependent solubility make calcium phosphate nanoparticles suitable for intracellular drug delivery. But one critical disadvantage of the calcium phosphate gene transfer system is the poor reproducibility compared with other nonviral systems [26]. The preparation of CP-pDNA complexes by co-precipitation method is difficult to control and has spontaneous tendency to form bulk precipitate, suffering from variations in the size and components of calcium phosphate and low transfection efficiency. The inoculations of magnesium salts and block copolymers have been proposed to inhibit crystal growth and regulate the crystal structure [27]. In the current study, OP-10/cyclohexane microemulsion was used as a microreactor for the precipitation of calcium phosphate in the presence of pDNA to regulate the crystal growth and particle size of CP-pDNA nanoparticles. Fig. 1a shows the morphology of nanoparticles, indicating irregular spherical profiles with the size of around 100 nm. The laser diffraction analysis showed that the size of CP-pDNA nanoparticles was 110 ± 35 nm, and the zeta potential was −2.6 ± 0.6 mV. The pDNA loading efficiency of CP-pDNA nanoparticles was determined to be 90.5 ± 3.2%.

Fig. 1b shows the XRD profile of CP-pDNA nanoparticles with a big broad peak centered at $2\theta = 31.8°$, a broad peak centered at $2\theta = 25.8°$, and smaller peaks centered at $2\theta = 28°$, 42°, and 47°, which are characteristic patterns of HA [28]. The broad peaks were seemingly designated as nonstoichiometric HA and low-crystalline apatitic phase, which may be a mixture of amorphous calcium phosphate and crystalline HA. Among calcium phosphate with different compositions, HA is the most stable and has low water solubility under neutral pH, but the solubility indicates a higher sensitivity to the acidic environments [29]. Through controlling the Ca/P feeding ratio of 5/3 and the reaction medium of pH 9.0, HA were formed in CP-pDNA nanoparticles.

With the purpose of investigating the level of protection, CP-pDNA nanoparticles were subjected to extensive DNase treatment followed by electrophoresis on 1% agarose gel. As shown in Fig. 1c, while free pDNA were completely digested by DNase treatment after 1 h, and pDNA absorbed on CP nanoparticles was digested after 2 h, pDNA encapsulated in CP-pDNA nanoparticles was totally protected after 4 h of DNase incubation. In the current study, two water-in-oil microemulsions allowed the precipitation of calcium phosphate in the presence of pDNA. The entrapment of pDNA into nanoparticles and the interaction between the pDNA and the calcium ions led to the protecting effect of CP-pDNA nanoparticles against DNase digestion.

ECs and SMCs were used to examine the cell viability and transfection levels after treated with CP-pDNA nanoparticles, compared with PEI–pDNA polyplexes and pDNA-absorbed CP nanoparticles. The mean diameter of pDNA polyplexes was 278 ± 42 nm, and the zeta potential was 4.1 ± 0.4 mV. As shown in Fig. 1d, PEI–pDNA polyplexes showed significantly lower cell viability compared to other groups. As we expected, free pDNA and pDNA absorbed on CP nanoparticles revealed significantly higher cell viability but lower transfection levels compared with other treatment (Fig. 1e). A slightly lower transfection efficiency was detected for CP-pDNA nanoparticles than that of PEI–pDNA polyplexes on both ECs and SMCs. The protein expression levels of SMCs were $(1.63 \pm 0.14) \times 10^5$ and $(2.30 \pm 0.19) \times 10^5$ RLU/mg protein after treated with CP-pDNA nanoparticles and PEI–pDNA polyplexes, respectively. Therefore, CP-pDNA nanoparticles indicated the desired balance of cytotoxicity and transfection efficiency, providing clinical relevance for angiogenic gene delivery for therapeutic vascularization and regeneration of functional tissues.

3.2. Characterization of pDNA-loaded electrospun fibers

Fig. 2a shows typical SEM morphologies of CP-pDNA-loaded electrospun fibers, indicating an average diameter of around 800 nm. The fibrous mats displayed a highly porous and randomly interconnected structure with an average porosity of 75.4%. pVEGF

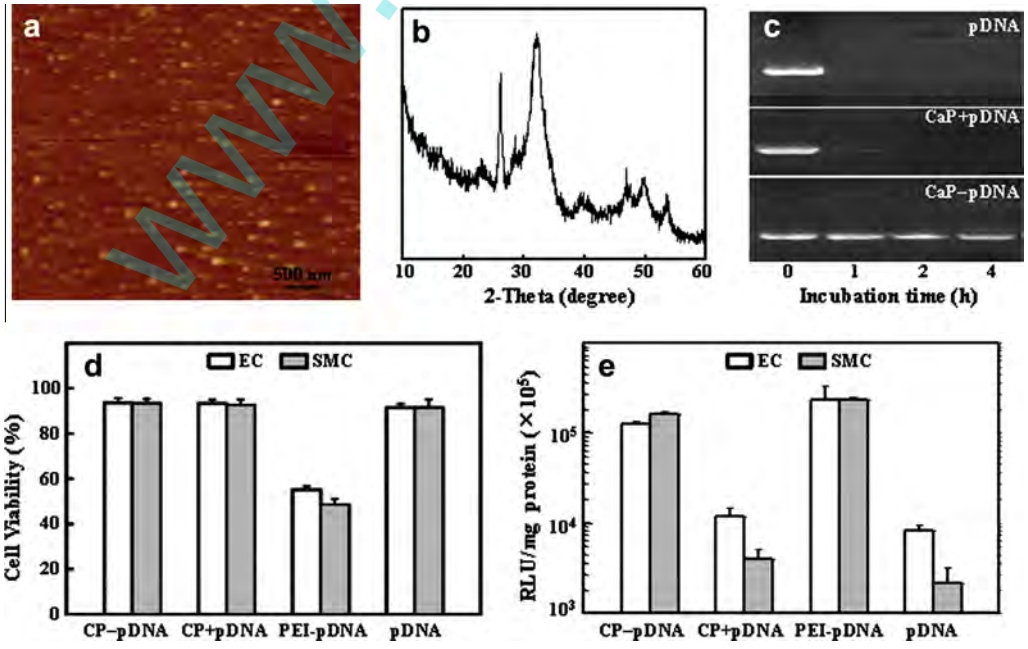

Fig. 1. Characterization of CP-pDNA nanoparticles. (a) AFM image and (b) XRD pattern of CP-pDNA nanoparticles; (c) Agarose gel electrophoresis analysis of pDNA extracted from CP-pDNA nanoparticles after incubation with DNase I for up to 4 h, compared with free pDNA, free pDNA-absorbed empty CP nanoparticles (CP + pDNA). (d) The viability and (e) transfection efficiency of ECs and SMCs after incubation with CP-pDNA nanoparticles, compared with CP + pDNA, PEI–pDNA polyplexes, and free pDNA ($n = 6$).

and pbFGF were labeled with DAPI and PI, respectively, to form fluorescent CP-pDNA nanoparticles. Fig. 2b shows the superimposing CLSM images of a single fiber under different exciting wavelength, indicating that both CP-pVEGF and CP-pbFGF nanoparticles were fully entrapped into electrospun fibers. Efficient encapsulation of therapeutics into fibers was one of the advantages of electrospinning process compared with other pDNA loading methods [17]. In current study, the pDNA entrapment efficiencies of Fv, Fb, and Fv-b fibers were determined to be 82.2 ± 2.0%, 81.9 ± 2.6%, and 77.1 ± 1.7%, respectively.

3.3. In vitro pDNA release from electrospun fibers

Fig. 3a summarizes the cumulative release profiles of pDNA from fibers, indicating an apparent initial burst during 24 h, followed by a sustained release over a prolonged period of time. For fibers without PEG inoculation, there was additional around 20% of sustained release during 4 weeks of incubation after the initial release. Owing to the size of around 100 nm and the interactions with matrix polymers, CP-pDNA nanoparticles did not diffuse appreciably in the release medium until the matrix polymers had been significantly degraded. The use of a fast degrading fiber matrix is possible to accelerate the release of nanoparticles, but the mechanic support of a scaffold for cell attachment and migration is essential for the regeneration of functional tissues. In the present study, 10% of PEG with M_w of 2, 4, and 6 kDa was blended into fiber matrices to modulate the pDNA release. The PEG inoculation was supposed to accelerate the hydrolyzation of fiber matrices, create microscopic holes in fibers after dissolution, and increase the contact area of matrix polymers with incubation media [17], leading to a release promotion of CP-pDNA nanoparticles from fibers. As shown in Fig. 3a, the molecular weight of PEG incorporated into the composite fibers had significant effects on the release behaviors of pDNA. The initial burst release of pDNA was around 10% for fibers containing PEG of 2 kDa, which increased to over 20% for those containing PEG of 6 kDa. Concomitantly, the total release of pDNA could be modulated within 13, 23, and over 30 days for fibers containing PEG of 2, 4, and 6 kDa, respectively. This can be attributed to the fact that the longer the molecular chains of PEG was, the larger channels and cavities were there after dissolution, which could promote medium exchange so as to release faster of CP-pDNA nanoparticles entrapped. As the periodicity of angiogenesis [30], 10% of PEG of 2 kDa was included into the matrix polymers to achieve a sustained release for 4 weeks, which was used in the following study.

Fig. 3b shows the agarose gel electrophoresis of pDNA released at different time points and free pDNA incubated in PBS as control. Bright bands were indicated in the sample pores, indicating the pDNA release in the form of CP-pDNA nanoparticles, which cannot move down in agarose gel electrophoresis. With the longer incubation periods, the amount of CP-pDNA nanoparticles decreased,

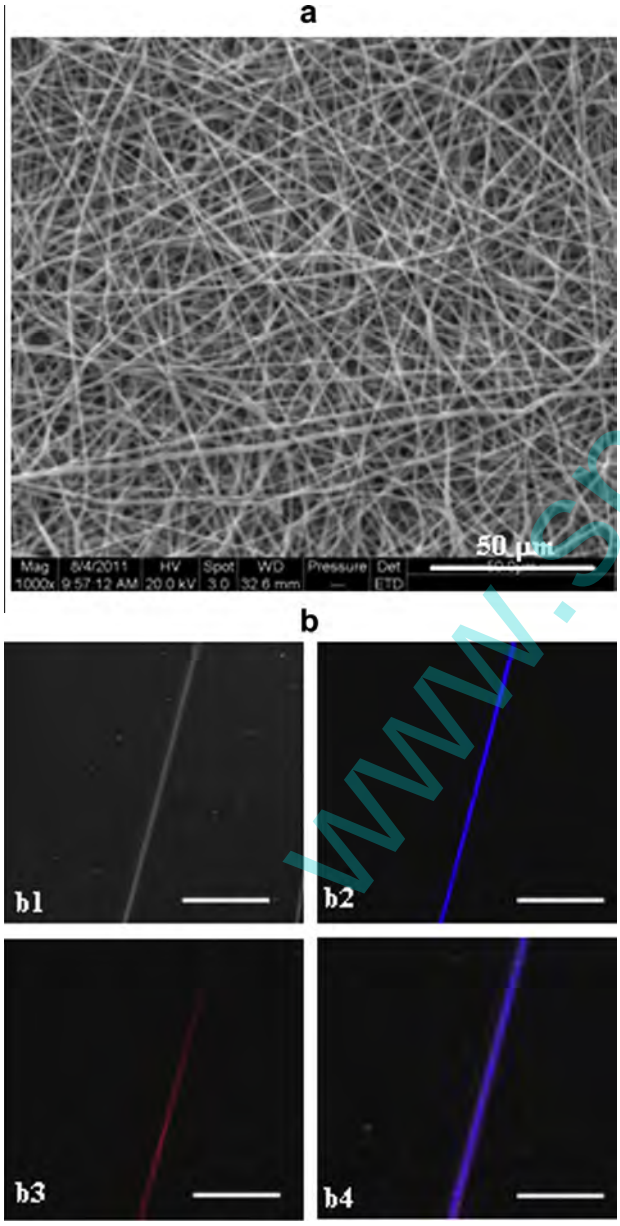

Fig. 2. Characterization of CP-pDNA nanoparticles-loaded electrospun fibers. (a) SEM image of Fv-b fibers. (b) Transmittance image (b1), CLSM images excited at 364 (b2) and 535 nm (b3), and superimposed CLSM images of Fv-b fibers excited at 364 and 535 nm (b4). Bars represent 10 μm.

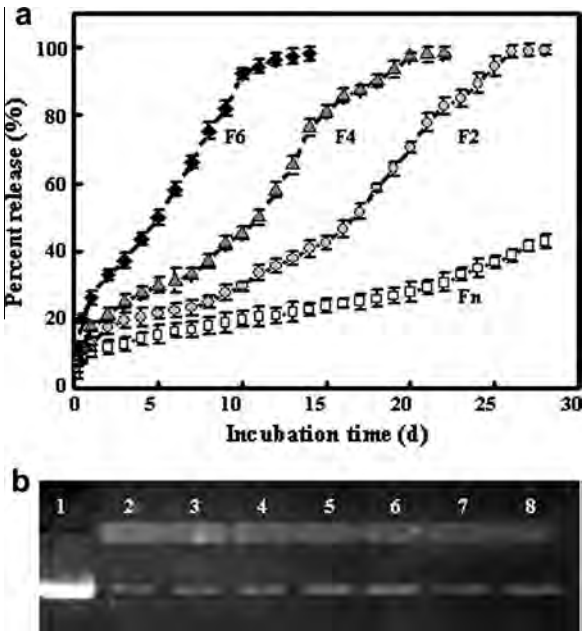

Fig. 3. (a) Percent release of pDNA from CP-pDNA nanoparticles-loaded fibers containing 10% PEG of 2 (F2), 4 (F4), and 6 kDa (F6), compared with those without PEG inoculation (Fn) after incubation in PBS, pH 7.4 at 37 °C (n = 3). (b) Agarose gel electrophoresis analysis of pDNA released from fibers at different time points with free pDNA incubated in PBS as control (lane 1). Lanes 2–8, pDNA released from fibers after incubation for 1, 3, 5, 7, 14, and 28 days.

while that of free pDNA increased. It was presumed that part of pDNA disassociated into the release medium from CP-pDNA nanoparticles released from fibers, and this process was intensified as the exchange of the release media with the time of release.

3.4. Cell attachment and viability on fibrous mats

The attachment and viability of ECs and SMCs were investigated on pDNA-loaded fibrous mats Fv, Fb, and Fv-b, CP-pDNA nanoparticles-infiltrated fibrous mats F_0 + v, F_0 + b, and F_0 + v-b and empty fibers F_0. As shown in Fig. 4a, compared with empty fibers, fibrous mats with CP-pDNA nanoparticles encapsulated or infiltrated indicated significantly lower attachment capabilities for both ECs and SMCs ($p < 0.05$), which may be due to the interactions with cell membrane and the slight cytotoxicity of CP-pDNA nanoparticles (Fig. 1d). In addition, the amounts of burst release from nanoparticles encapsulated fibers were lower than those diffused out from nanoparticles-infiltrated fibrous mats, leading to a slightly higher cell attachment on Fv, Fb, and Fv-b fibers. In our previous study, the attachment ability of ECs on fibrous mats with PEI–pDNA polyplexes infiltrated was around 40–50% of that on TCP [19]. However, there was over 65% of relative cell attachment after incubation with nanoparticles-infiltrated fibrous mats, reflecting the low cytotoxicity of CP-pDNA nanoparticles.

As shown in Fig. 4a, the growth behaviors on empty fibers were almost identical to those TCP for both ECs and SMCs. In our previous study [19], during the initial 3-day incubation, apparent decreases in the cell viability were determined on fibrous mats containing PEI–pDNA polyplexes, owing to the cytotoxicity of pDNA polyplexes and persistent cell transfection. However, the relative cell viabilities showed no significant difference during 3 days of incubation with fibrous mats containing CP-pDNA nanoparticles ($p > 0.05$). For these pDNA-loaded scaffolds, the growth rate of cells depended on the competition of cytotoxicity of transfection agents and the growth promotion effect of growth factors secreted by transfect cells [19]. The expression of bFGF and VEGF could promote the cell proliferation, resulting in gradual increases during the following incubation time period for both ECs and SMCs (Fig. 4a). Moreover, compared to that of CP-pDNA nanoparticles-infiltrated fibrous mats, the sustainable release of CP-pDNA nanoparticles from Fv, Fb, and Fv-b fibers was supposed to keep high transfection efficiency and continuous growth factor expression, resulting in a significantly higher increase in the growth rate during the last several days. After 7 days of incubation, the relative viabilities of ECs on Fv and Fv-b fibrous mats reached around 90% compared with TCP, which was significantly higher than that of empty fibers F_0 (around 80%) and fibers with PEI–pDNA polyplexes entrapped (around 60%) ($p < 0.05$) [19]. In the meantime, the relative viabilities of SMCs on CP-pDNA nanoparticles encapsulated fibers indicated a steadily increase after 1 day incubation and slightly higher relative cell viabilities than that of empty fibers after 7 days. It was concluded that the gradual release of CP-pDNA nanoparticles from fibers had the benefits in promoting the cell attachment and viabilities.

3.5. Transfection efficiency of cells on fibrous mats

The transfection efficiency of pVEGF and pbFGF was determined by the expression of fusion proteins of VEGF/eGFP and bFGF/eGFP, respectively. As shown in Fig. 4b, significantly higher transfection levels were observed on days 3 and 5 after incubation with CP-pDNA nanoparticles-infiltrated fibrous mats than those with pDNA-encapsulated mats for both ECs and SMCs ($p < 0.05$). However, the cell transfection efficiency on Fv, Fb, and Fv-b fibrous

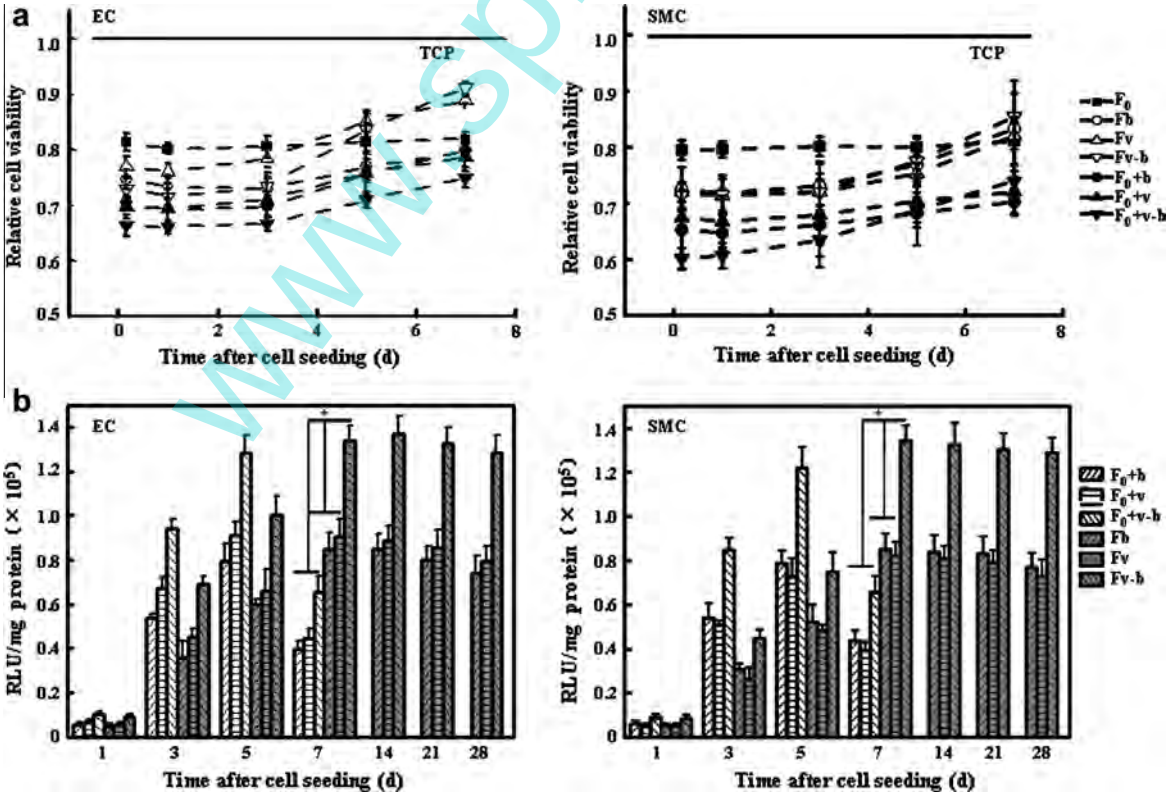

Fig. 4. (a) Cell attachment after 4 h seeding and cell viability at different time points after incubation of ECs and SMCs on CP-pDNA nanoparticles encapsulated fibrous mats Fv, Fb and Fv-b, CP-pDNA nanoparticles-infiltrated fibrous mats F_0 + v, F_0 + b, and F_0 + v-b, and empty fibers F_0, compared with TCP (solid lines) ($n = 6$). (b) Transfection efficiency of ECs and SMCs after incubation with Fv, Fb and Fv-b fibrous mats, compared with F_0 + v, F_0 + b, and F_0 + v-b fibrous mats ($n = 6$, $^*p < 0.05$).

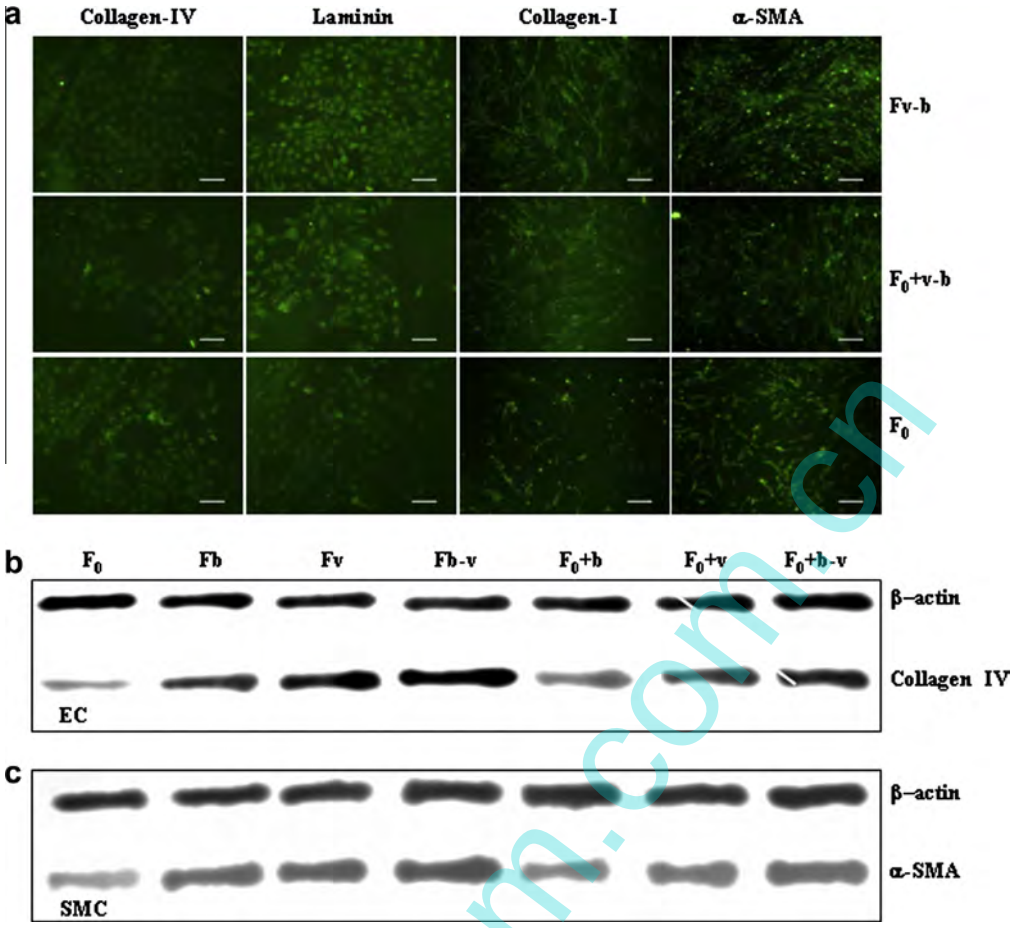

Fig. 5. (a) Immunofluorescent staining images of collagen IV and laminin expressions by ECs, and collagen I and α-SMA by SMCs after incubation for 7 days with Fv-b, F_0 + v-b and F_0 fibrous mats. Bars represent 20 μm. (b) Western blotting assay of collagen IV expressions by ECs and (c) α-SMA by SMCs after incubation for 7 days with Fv, Fb and Fv-b fibrous mats, compared with F_0, F_0 + v, F0 + b, and F_0 + v-b fibrous mats. Total proteins were prepared from cell lysate, and α-actin was used as protein loading control.

mats increased gradually during the incubation period and became significantly higher than those on F_0 + v, F_0 + b, and F_0 + v-b fibrous mats on day 7 after incubation ($p < 0.05$). This may be due to the dissociation and consumption of CP-pDNA nanoparticles in the cell-culture media for F_0 + v, F_0 + b, and F_0 + v-b fibrous mats. Another reason may be the decrease in physiological stability of CP nanoparticles [31]. The formation of larger aggregates cannot be easily internalized into cells via the endocytotic process, resulting in low transfection efficiency in biological systems. In addition, the transfection of CP-pDNA nanoparticles did not lead to the incorporation of DNA into the host genome, and the transient transfection should be diluted with the increased viability of cells. So, the transfection levels of ECs and SMCs were highest on day 5 after incubation with CP-pDNA nanoparticles-infiltrated fibrous mats, and significant decreases were observed during the following incubation period (Fig. 4b). In contrast, the gradual release of CP-pDNA nanoparticles from Fb, Fv, and Fb-v fibers kept the intact structure and maintained the transfection capabilities, leading to a persistent and incremental protein expression.

As shown in Fig. 4b, there was a similar phenomenon at each time points, that is to say, the transfection efficiency of groups treated with both pVEGF and pbFGF was higher, regardless of F_0 + v-b and Fv-b, than that of the groups treated with individual pDNA. No significant difference in the transfection levels was detected between pVEGF and pbFGF-loaded fibers during the incubation period ($p > 0.05$). However, after 7 days of incubation, there was an almost 50–70% increase in the GFP expression for Fv-b than Fv fibers, at $(1.34 \pm 0.07) \times 10^5$ and $(0.91 \pm 0.08) \times 10^5$ RLU/mg protein for ECs, and $(1.34 \pm 0.07) \times 10^5$ and $(0.82 \pm 0.06) \times 10^5$ RLU/mg protein for SMCs, respectively. The difference in the transfection efficiency should be ascribed to the expression of bFGF/eGFP for Fv-b fibers.

The gradual release of CP-pDNA nanoparticles from fibers was supposed to transfect cells and stimulate growth factor secretion continuously. In the present study, ECs and SMCs were removed from fibrous scaffolds by trypsinization after 7 days of culture, and another batch of cells was seeded on the recovered fibrous mats and incubated for additional 7 days. The cell depletion and seeding processes were repeated, and the cell transfection efficiency was determined after 14, 21, and 28 days of incubation. There was no significant decrease in the transfection levels on day 28 compared to that on day 7 after incubation (Fig. 4b), indicating the capabilities of fibrous scaffolds with CP-pDNA nanoparticles encapsulated to extend the availability of growth factors at effective levels within local tissue environment.

3.6. The ECM secretion of cells on fibrous mats

The substantial function of endothelial cells is the production of basal lamina for microvessel, which is composed of a number of macromolecules, including collagen, proteoglycans, and glycoproteins [32]. The important role of vascular smooth muscle cells is to maintain the integrity and function of mature blood vessels by expression of smooth muscle-specific variants of cytoskeletal and

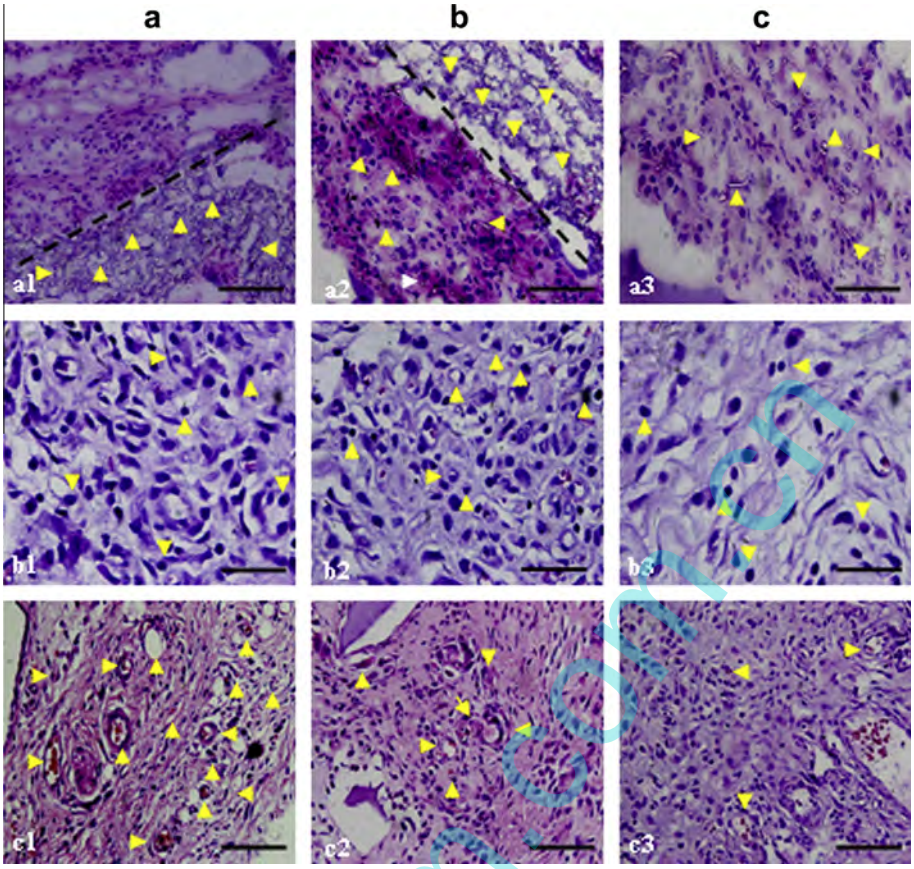

Fig. 6. (A) Fiber residuals and cell infiltration observed by HE staining after implantation of Fv-b fibrous mats for 1 (a1), 2 (a2), and 4 weeks (a3). Arrow heads indicate the fiber residuals, and dotted lines the interface of cell infiltration. Bars represent 50 μm. (B) HE staining of inflammatory reactions at week 1 after implantation of Fv-b (b1), F_0 + v-b (b2), and F_0 fibrous mats (b3). Arrow heads indicate inflammatory cells. Bars represent 20 μm. (C) HE staining for blood vessel formation at week 4 after implantation of Fv-b (c1), F_0 + v-b (c2), and F_0 fibrous mats (c3). Arrow heads indicate vessels with filled red blood cells. Bars represent 50 μm.

contractile proteins such as α-SMA, myosin, collagen I, and elastin [33]. In the present study, collagen IV and laminin secreted by ECs and collagen I and α-SMA by SMCs were evaluated after 7 days of culture with pDNA-loaded fibers. Fig. 5a shows typical images of immunofluorescent staining. Strong expression of extracellular proteins was indicated for both ECs and SMCs. Fig. 5b summarizes the Western blotting results of collagen IV and α-SMA expressions, using β-actin as protein loading control. As shown in the band density, the amount of collagen IV and α-SMA extracted from cells treated with Fv-b fibers was significantly higher than those from other fibers, which should be ascribed to the fact that VEGF and bFGF expressed simultaneously. The ECM secretion reflected results similar to the cell viability and transfection tests (Fig. 4), indicated a continuous and slow release of CP-pDNA nanoparticles from fibers enhanced the expression of pDNA encoding growth factors. In addition, compared with the promotion effect of bFGF on both ECs and SMCs [34], VEGF was beneficial to the proliferation of ECs, but could not promote or inhibit SMCs to grow nearly [35]. As shown in Fig. 5b, the band intensity of collagen IV for Fv-treated ECs was higher than that of Fb, while there was no apparent difference for those of SMCs.

3.7. Histological staining after subcutaneous implantation

To evaluate the blood vessel formation enhanced by pDNA-loaded fibrous mats, the scaffolds with surrounding tissues were explanted at different intervals, and histological studies were executed by HE and IHC staining on tissue sections. Fig. 6 summarized the results of HE staining on frozen sections to examine the fiber degradation, inflammatory reaction, and blood vessel formation. Fig. 6A shows the tissue infiltration into fibrous scaffolds and fiber residuals after implantation, indicating that fibers were degraded and absorbed along with cell migration and tissue ingrowth. There was a clear border between Fv-b fibers and tissues at 1 week (Fig. 6a1). After 2 weeks of implantation, tissue ingrowth occupied more of the implanted scaffolds although the border existed (Fig. 6a2), while there was no integral polymeric fiber, but fiber fragment observed in the histological sections at week 4 after operation (Fig. 6a3).

In our previous study, the implantation of fibrous mats with PEI–pDNA polyplexes included induced strong inflammation both between fibrous layers and at the interface of fibrous mats with penetrated tissues, and necrotic tissue was observed followed by scar formation [19]. Fig. 6B shows the typical HE staining images of infiltrated tissues at 1 week after implantation, indicating inflammatory cells surrounding the implanted fibers. HE staining of tissues retrieved after 4 weeks of implantation revealed no inflammatory cell remaining, indicating that CP-pDNA nanoparticles caused much weaker tissue reaction than PEI–pDNA polyplexes. Blood vessels were formed after cells infiltrated into implants and were arranged into a circular structure, and the vascular density of Fv-b was significantly higher than that of F_0 + v-b and empty fibers F_0 (Fig. 6C), indicating that the gradual release of CP-pDNA nanoparticles and sustained express of growth factors promoted angiogenesis in a long time. In addition, the vessel-like structures were filled with red blood cells, suggesting the integration of the newly formed vessels with native vasculature. To summarize, HE staining results revealed the gradual degradation of fibrous

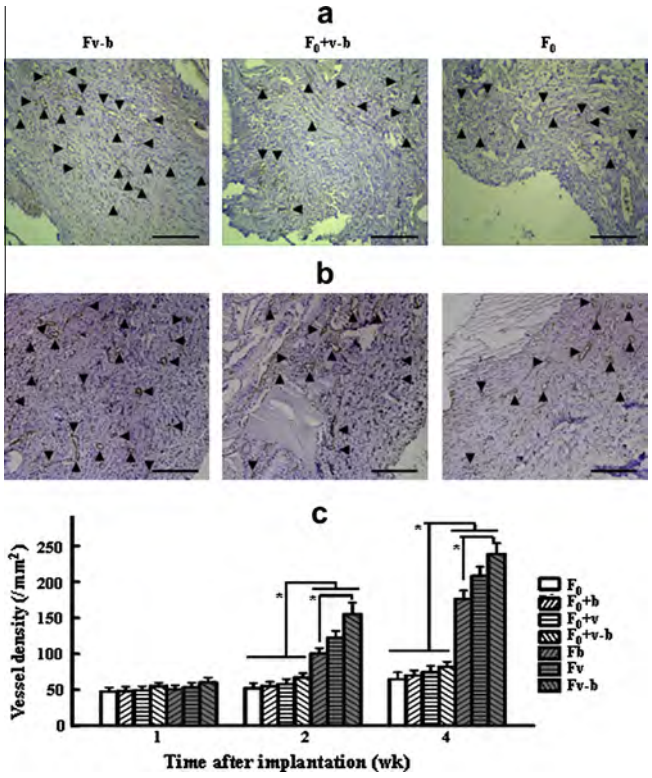

Fig. 7. IHC staining images for CD31 (a) and collagen IV expressions (b) of tissue explants treated with Fv-b, F_0 + v-b and F_0 fibrous mats for 4 weeks. Arrow heads indicate collagen IV–positive vessels with morphological circumference. Bars represent 100 μm. (c) Quantitative counts of collagen IV–positive vessels and normalized to tissue area (# vessels/mm^2) after implantation for 1, 2 and 4 weeks of Fv, Fb and Fv-b fibrous mats, compared with F_0, F_0 + v, F_0 + b and F_0 + v-b fibrous mats. $^*p < 0.05$.

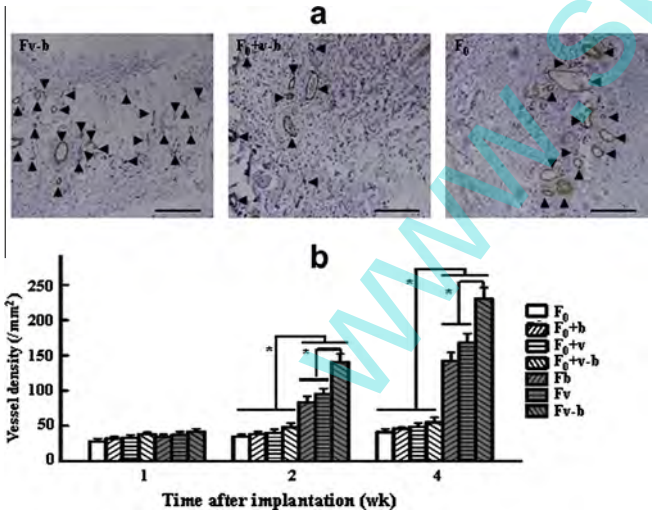

Fig. 8. (a) IHC staining images for α-SMA expressions of tissue explants treated with Fv-b, F_0 + v-b and F_0 fibrous mats for 4 weeks. Arrow heads indicate α-SMA–positive vessels with morphological circumference. Bars represent 100 μm. (b) Quantitative counts of α-SMA–positive vessels and normalized to tissue area (# vessels/mm^2) after implantation for 1, 2 and 4 weeks of Fv, Fb and Fv-b fibrous mats, compared with F_0, F_0 + v, F_0 + b and F_0 + v-b fibrous mats. $^*p < 0.05$.

scaffolds followed by cellular infiltration, and the encapsulation of CP-pDNA nanoparticles into fibers induced few inflammatory reaction and enhanced the growth of blood vessels.

3.8. IHC staining of collagen IV and α-SMA

Mature blood vessels are characterized by a layer of endothelial cells surrounded by smooth muscle cells and pericytes in the walls. CD31 was used primarily to demonstrate the presence of endothelial cells in histological tissue sections, and the deposition of collagen IV indicated a similar distribution of endothelial cells [36], while α-SMA was usually used to study the level of maturation of the newly formed blood vessels [37]. To investigate the vascularization process, tissue sections were stained with anti-CD31, anti-collagen type IV and anti-α-SMA after 1, 2, and 4 weeks of implantation.

Fig. 7 shows IHC staining results of CD31 and collagen IV, indicating a circular morphology in all the tissue sections. The collagen IV-positive staining was used to manually determine the total number of blood vessels [38]. As shown in Fig. 7, there was no significant difference in the vessel densities of all the test groups after 1 week of implantation ($p > 0.05$). A slight increase in the vessel densities was observed at week 2 after implantation of F_0 + v, F_0 + b, and F_0 + v-b fibers, but no significant difference was observed in the vessel density compared to empty fibers at each time point ($p > 0.05$). The positively stained vessels gradually increased after implantation of Fv, Fb, and Fv-b fibers, at 208 ± 16, 176 ± 12, and 239 ± 15 vessels/mm^2 at week 4, respectively. Fv-b fibrous scaffolds indicated significantly higher vessel densities than other groups ($p < 0.05$).

Fig. 8 shows IHC staining images for α-SMA expression of tissue explants, indicating the existence of α-SMA-secreting cells, such as smooth muscle cells and pericytes in the walls of newly formed blood vessels. α-SMA positive staining was used as a marker for mature blood vessels [38], and the quantitative results of mature microvessel densities after 1, 2, and 4 weeks of implantation are shown in Fig. 8b. The densities of mature blood vessels were around 40 vessels/mm^2 for all the experiment groups after 1 week of implantation. There was no significant difference in the α-SMA positive staining at weeks 2 and 4 compared with that at week 1 after implantation of CP-pDNA nanoparticles-infiltrated fibers or empty fibers ($p > 0.05$). However, the microvessel density indicated a steady increase after implantation of fibers encapsulated with CP-pDNA nanoparticles. At week 4, there were 168 ± 13, 142 ± 12, and 230 ± 16 vessels/mm^2 for Fv, Fb, and Fv-b fibers, respectively.

As shown in Figs. 7 and 8, compared with those of F_0 + v, F_0 + b, and F_0 + v-b fibers, significantly higher densities of blood vessels were generated after 2 and 4 weeks of implantation of Fv, Fb, and Fv-b fibers ($p < 0.05$). This was in accordance with the higher cell viability, stronger protein expression (Fig. 4), and ECM secretion (Fig. 5) after incubation of ECs and SMCs on fibers encapsulated with CP-pDNA nanoparticles than those with nanoparticles infiltrated. It was indicated that the sustained release of pDNA ensured the long-term availability of signals at effective levels within the local tissue microenvironment. In addition, angiogenesis is a complex, multi-step process, and distinct factors are involved in each step [39]. Therefore, delivery of multiple factors may be required to increase the efficacy of angiogenesis. VEGF can stimulate the proliferation, morphogenesis, and differentiation of vascular endothelial cells and strengthen the permeability of blood vessel [40]. bFGF, another important growth factor, not only cause the proliferation, morphogenesis, and differentiation of many types of cells, but also can facilitate the recruitment of smooth muscle cells or pericytes [41], which form a single cell layer around the newly formed capillary, necessary to mature the blood vessels and to protect them from degradation. As shown in Figs. 7 and 8, Fv-b fibers containing both pbFGF and pVEGF led to significantly higher densities of blood vessels and mature vessels than those of Fv and Fb after 2 and 4 weeks of implantation ($p < 0.05$). Similar

results were also reflected in the collagen secretion by ECs and α-SMA secretion by SMCs (Fig. 5). It should be noted that the sustained and localized delivery of pbFGF accelerated the maturation process of blood vessels. After 2 and 4 weeks of implantation, the difference between Fv-b and Fv or Fb in the densities of mature blood vessels (Fig. 8) was larger than that in microvessel densities (Fig. 7). It was demonstrated that the combined treatment promoted the formation of vascular network and induced the rapid generation of mature blood vessels. Moreover, compared with that of PEI–pDNA polyplexes, the sustained release of CP-pDNA nanoparticles from electrospun fibers caused significantly higher cell viability (Fig. 4) and much weaker inflammation reactions in subcutaneous tissues (Fig. 6). Therefore, the integration of CP-pDNA nanoparticles with loadings of multiple plasmids into tissue engineering scaffolds should provide clinical relevance for therapeutic vascularization and regeneration of functional tissues.

4. Conclusion

Electrospun fibers with loadings of CP-pDNA nanoparticles were evaluated in the current study to promote the generation of blood vessels. Compared with PEI–pDNA polyplexes, CP-pDNA nanoparticles showed significantly higher cell viability, comparable transfection efficiency and less inflammation reaction after implantation into animals. The inoculation of PEG with 2 kDa into fiber matrices achieved a sustained release for 4 weeks to match the duration for the formation of mature blood vessel. The localized and gradual release of pDNA facilitated the proliferation, gene transfection, and ECM secretion of ECs and SMCs and enhanced the generation of blood vessels. The delivery of both pVEGF and pbFGF resulted in higher ECM secretion and significantly higher densities of mature blood vessels than that of individual plasmid. Although there are many challenges that need to be addressed, the integration of CP-pDNA nanoparticles with loadings of multiple plasmids into electrospun fibrous scaffolds should provide clinical relevance for getting fully vascularized in engineered tissues and regenerating promptly blood vessel substitutes.

Acknowledgements

This work was supported by National Basic Research Program of China (973 Program, 2012CB933602), National Natural Science Foundation of China (51073130 and 21274117), Specialized Research Fund for the Doctoral Program of Higher Education (20120184110004), and Fundamental Research Funds for the Central Universities (SWJTU11ZT10).

References

[1] E.C. Novosel, C. Kleinhans, P.J. Kluger, Vascularization is the key challenge in tissue engineering, Adv. Drug Deliv. Rev. 63 (2011) 300–311.
[2] J.K. Tessmar, A.M. Göpferich, Matrices and scaffolds for protein delivery in tissue engineering, Adv. Drug Deliv. Rev. 59 (2007) 274–291.
[3] S.M. Anderson, S.N. Siegman, T. Segura, The effect of vascular endothelial growth factor (VEGF) presentation within fibrin matrices on endothelial cell branching, Biomaterials 32 (2011) 7432–7443.
[4] A. Des Rieux, B. Ucakar, B.P. Mupendwa, D. Colau, O. Feron, P. Carmeliet, P. Véronique, 3D systems delivering VEGF to promote angiogenesis for tissue engineering, J. Control. Release 150 (2011) 272–278.
[5] K. Fu, A.M. Klibanov, R. Langer, Protein stability in controlled release systems, Nat. Biotechnol. 18 (2000) 24–25.
[6] J.H. Jang, C.B. Rives, L.D. Shea, Plasmid delivery in vivo from: transgene expression and cellular transfection, Mol. Ther. 12 (2005) 475–483.
[7] R. Guo, S. Xu, L. Ma, A. Huang, C. Gao, The healing of full-thickness burns treated by using plasmid DNA encoding VEGF-165 activated collagen–chitosan dermal equivalents, Biomaterials 32 (2011) 1019–1031.
[8] S. Neumann, A. Kovtun, I.D. Dietzel, M. Epple, R. Heumann, The use of size-defined DNA-functionalized calcium phosphate nanoparticles to minimise intracellular calcium disturbance during transfection, Biomaterials 30 (2009) 6794–6802.
[9] S.D. Patil, D.G. Rhodes, D.J. Burgess, DNA-based therapeutics and DNA delivery systems: a comprehensive review, AAPS J. 7 (2005) 61–77.
[10] M. Okazaki, Y. Yoshida, S. Yamaguchi, M. Kaneno, J.C. Elliott, Affinity binding phenomena of DNA onto apatite crystals, Biomaterials 22 (2001) 2459–2464.
[11] V.L. Truong-Le, S.M. Walsh, E. Schweibert, H.Q. Mao, W.B. Guggino, J.T. August, K.W. Leong, Gene transfer by DNA–gelatin nanospheres, Arch. Biochem. Biophys. 361 (1999) 47–56.
[12] M. Stubbs, P.M. McSheehy, J.R. Griffiths, C.L. Bashford, Causes and consequences of tumour acidity and implications for treatment, Mol. Med. Today 6 (2000) 15–19.
[13] C.M. Curtin, G.M. Cunniffe, F.G. Lyons, K. Bessho, G.R. Dickson, G.P. Duffy, F.J. O'Brien, Innovative collagen nano-hydroxyapatite scaffolds offer a highly efficient non-viral gene delivery platform for stem cell-mediated bone formation, Adv. Mater. 24 (2012) 749–754.
[14] A. Greiner, J.H. Wendorff, Electrospinning: a fascinating method for the preparation of ultrathin fibers, Angew. Chem. Int. Ed. 46 (2007) 5670–5703.
[15] S. Sakai, Y. Yamada, T. Yamaguchi, T. Ciach, K. Kawakami, Surface immobilization of poly(ethyleneimine) and plasmid DNA on electrospun poly(L-lactic acid) fibrous mats using a layer-by-layer approach for gene delivery, J. Biomed. Mater. Res. A 88 (2009) 281–287.
[16] H. Nie, C.H. Wang, Fabrication and characterization of PLGA/HAp composite scaffolds for delivery of BMP-2 plasmid DNA, J. Control. Release 120 (2007) 111–121.
[17] Y. Yang, X.H. Li, L. Cheng, S.H. He, J. Zou, F. Chen, Z.B. Zhang, Core-sheath-structured fibers with pDNA polyplex loadings for optimal release profile and transfection efficiency as potential tissue engineering scaffolds, Acta Biomater. 7 (2011) 2533–2543.
[18] Y. Yang, T. Xia, F. Chen, W. Wei, C. Liu, S.H. He, X.H. Li, Electrospun fibers with plasmid bFGF polyplexes loadings promote skin wound healing in diabetic rats, Mol. Pharm. 9 (2012) 48–58.
[19] S.H. He, T. Xia, H. Wang, L. Wei, X.M. Luo, X.H. Li, Multiple releases of polyplexes of plasmids VEGF and bFGF from electrospun fibrous scaffolds towards regeneration of mature blood vessels, Acta Biomater. 8 (2012) 2659–2669.
[20] V.V. Sokolova, I. Radtke, R. Heumann, M. Epple, Effective transfection of cells with multi-shell calcium phosphate-DNA nanoparticles, Biomaterials 27 (2006) 3147–3153.
[21] M. Presta, P. Dell'Era, S. Mitola, E. Moroni, R. Ronca, M. Rusnati, Fibroblast growth factor/fibroblast growth factor receptor system in angiogenesis, Cytokine Growth Factor Rev. 16 (2005) 159–178.
[22] X.H. Li, Y.H. Zhang, W.X. Jia, X.M. Deng, Z.T. Huang, Influence of process parameters on the protein stability encapsulated in poly-DL-lactide-poly(ethylene glycol) microspheres, J. Control. Release 68 (2000) 4152.
[23] T.T. Morgan, H.S. Muddana, E.I. Altinoglu, S.M. Rouse, A. Tabaković, T. Tabouillot, T.J. Russin, S.S. Shanmugavelandy, P.J. Butler, P.C. Eklund, J.K. Yun, M. Kester, J.H. Adair, Encapsulation of organic molecules in calcium phosphate nanocomposite particles for intracellular imaging and drug delivery, Nano Lett. 8 (2008) 4108–4115.
[24] X.L. Zhu, W.G. Cui, X.H. Li, Y. Jin, Electrospun fibrous mats with high porosity as potential scaffolds for skin tissue engineering, Biomacromolecules 9 (2008) 1795–1801.
[25] I. Masaki, Y. Yonemitsu, A. Yamashita, S. Sata, M. Tanii, K. Komori, K. Nakagawa, X. Hou, Y. Nagai, M. Hasegawa, K. Sugimachi, K. Sueishi, Angiogenic gene therapy for experimental critical limb ischemia: acceleration of limb loss by overexpression of vascular endothelial growth factor 165 but not of fibroblast growth factor-2, Circ. Res. 90 (2002) 966–973.
[26] K.D. Kianoush, R.M. Mohamaad, R. Ladan, M. Mehrdad, Calcium based non-viral gene delivery: an overview of methodology and applications, Acta Med. Iran. 48 (2010) 133–141.
[27] Y. Kakizawa, K. Kataoka, Block copolymer self-assembly into monodispersive nanoparticles with hybrid core of antisense DNA and calcium phosphate, Langmuir 18 (2002) 4539–4543.
[28] H.W. Kim, J.H. Song, H.E. Kim, Nanofiber generation of gelatin–hydroxyapatite biomimetics for guided tissue regeneration, Adv. Funct. Mater. 15 (2005) 1988–1994.
[29] J.C. Elliott, Structure and Chemistry of the Apatites and Other Calcium Orthophosphates, Elsevier, Amsterdam, The Netherlands, 1994, pp. 1–12.
[30] F.R. Formiga, B. Pelacho, E. Garbayo, G. Abizanda, J.J. Gavira, T. Simon-Yarza, M. Mazo, E. Tamayo, C. Jauquicoa, C. Ortiz-de-Solorzano, F. Prósper, M.J. Blanco-Prieto, Sustained release of VEGF through PLGA microparticles improves vasculogenesis and tissue remodeling in an acute myocardial ischemia–reperfusion model, J. Control. Release 147 (2010) 30–37.
[31] S.L. Zhang, J. Li, G. Lykotrafitis, G. Bao, S. Suresh, Size-dependent endocytosis of nanoparticles, Adv. Mater. 21 (2009) 419–424.
[32] C.M. Kelleher, S.E. McLean, R.P. Mecham, Vascular extracellular matrix and aortic development, Curr. Top. Dev. Biol. 62 (2004) 153–188.
[33] C. Adelöw, T. Segura, J.A. Hubbell, P. Frey, The effect of enzymatically degradable poly(ethylene glycol) hydrogels on smooth muscle cell phenotype, Biomaterials 29 (2008) 314–326.
[34] M. Fujita, M. Ishihara, M. Simizu, K. Obara, T. Ishizuka, Y. Saito, H. Yura, Y. Morimoto, B. Takase, T. Matsui, M. Kikuchi, T. Maehara, Vascularization in vivo caused by the controlled release of fibroblast growth factor-2 from an injectable chitosan/non-anticoagulant heparin hydrogel, Biomaterials 25 (2004) 699–706.
[35] L. Wei, J. Lin, C. Cai, Z. Fang, W. Fu, Drug-carrier/hydrogel scaffold for controlled growth of cells, Eur. J. Pharm. Biopharm. 78 (2011) 346–354.

[36] A.P. Taylor, M. Rodriguez, K. Adams, D.M. Goldenberg, R.D. Blumenthal, Altered tumor vessel maturation and proliferation in placenta growth factorproducing tumor: potential relationship to post-therapy tumor angiogenesis and recurrence, Int. J. Cancer 105 (2003) 158–164.
[37] G.D. Yancopoulos, S. Davis, N.W. Gale, J.S. Rudge, S.J. Wiegand, J. Holash, Vascular-specific growth factors and blood vessel formation, Nature 407 (2000) 242–248.
[38] S.T. Nillesen, P.J. Geutjes, R. Wismans, J. Schalkwijk, W.F. Daamen, T.H. van Kuppevelt, Increased angiogenesis and blood vessel maturation in acellular collagen–heparin scaffolds containing both FGF2 and VEGF, Biomaterials 28 (2007) 1123–1131.
[39] P. Carmeliet, Angiogenesis in health and disease, Nat. Med. 9 (2003) 653–660.
[40] R.C. Hendel, T.D. Henry, K. Rocha-Singh, J.M. Isner, D.J. Kereiakes, F.J. Giordano, M. Simons, R.O. Bonow, Effect of intracoronary recombinant human vascular endothelial growth factor on myocardial perfusion: evidence for a dose-dependent effect, Circulation 101 (2000) 118–121.
[41] M. Klaqsbrun, The fibroblast growth factor family: structural and biological properties, Prog. Growth Factor Res. 1 (1989) 207–235.